Cerebral Cortex Advance Access published February 12, 2010

Cerebral Cortex
doi:10.1093/cercor/bhq011

Dissociable Connectivity within Human Angular Gyrus and Intraparietal Sulcus: Evidence from Functional and Structural Connectivity

Lucina Q. Uddin[1], Kaustubh Supekar[1,2], Hitha Amin[1], Elena Rykhlevskaia[1,3,4], Daniel A. Nguyen[1], Michael D. Greicius[4] and Vinod Menon[1,4,5]

[1]Department of Psychiatry and Behavioral Sciences, Stanford University School of Medicine, Stanford, CA 94304, USA, [2]Graduate Program in Biomedical Informatics, Stanford University School of Medicine, Stanford, CA 94305, USA, [3]Department of Psychology, Stanford University, Stanford, CA 94305, USA, [4]Department of Neurology and Neurological Sciences, Stanford University School of Medicine, Stanford, CA 94305, USA and [5]Program in Neuroscience, Stanford University School of Medicine, Stanford, CA 94304, USA

Address correspondence to Lucina Q. Uddin, 780 Welch Road, Room 201, Stanford, CA 94304, USA. Email: lucina@stanford.edu

The inferior parietal lobule (IPL) of the human brain is a heterogeneous region involved in visuospatial attention, memory, and mathematical cognition. Detailed description of connectivity profiles of subdivisions within the IPL is critical for accurate interpretation of functional neuroimaging studies involving this region. We separately examined functional and structural connectivity of the angular gyrus (AG) and the intraparietal sulcus (IPS) using probabilistic cytoarchitectonic maps. Regions-of-interest (ROIs) included anterior and posterior AG subregions (PGa, PGp) and 3 IPS subregions (hIP2, hIP1, and hIP3). Resting-state functional connectivity analyses showed that PGa was more strongly linked to basal ganglia, ventral premotor areas, and ventrolateral prefrontal cortex, while PGp was more strongly connected with ventromedial prefrontal cortex, posterior cingulate, and hippocampus—regions comprising the default mode network. The anterior-most IPS ROIs, hIP2 and hIP1, were linked with ventral premotor and middle frontal gyrus, while the posterior-most IPS ROI, hIP3, showed connectivity with extrastriate visual areas. In addition, hIP1 was connected with the insula. Tractography using diffusion tensor imaging revealed structural connectivity between most of these functionally connected regions. Our findings provide evidence for functional heterogeneity of cytoarchitectonically defined subdivisions within IPL and offer a novel framework for synthesis and interpretation of the task-related activations and deactivations involving the IPL during cognition.

Keywords: attention, Brodmann area 39, default mode network, inferior parietal lobule, mathematical cognition

Introduction

The posterior parietal cortex (PPC), and in particular the inferior parietal lobule (IPL), is a brain region which is engaged in a wide variety of cognitive domains ranging from visuospatial attention (Corbetta and Shulman 2002) to episodic memory (Cabeza et al. 2008) and mathematical cognition (Dehaene et al. 2004). Its involvement in multiple cognitive operations suggests that the region is highly heterogeneous, and may be further subdivided into functional areas. The subdivisions of the human IPL are not well understood, and their relation to functional and structural connectivity is completely unknown. Autoradiographic tracer studies in the macaque brain have demonstrated a rostro-caudal gradient of connectivity within the IPL, with rostral IPL connected to ventral premotor areas and caudal IPL connected to Brodmann areas 44 and 45 (Petrides and Pandya 2009). However, the extent to which the human IPL can be considered strictly homologous to its monkey counterpart is a matter of debate. While Brodmann's initial characterization of the region led him to conclude that the human IPL consists of novel cortical areas not present in the monkey, others have argued that the IPL is similar across both species (Husain and Nachev 2007). Thus, it is unclear to what degree monkey anatomical tracer studies can be extrapolated to understanding these pathways in the human brain.

The human IPL consists of 3 prominent functional and anatomical subdivisions, the angular gyrus (AG), the supramarginal gyrus, and the banks of the intraparietal sulcus (IPS). Situated at the junction of the temporal, parietal, and occipital lobes, the AG is a heteromodal region. Previous functional neuroimaging studies have focused on its role in language and semantic processing (Binder et al. 2009; Brownsett and Wise 2009) or spatial attention and orienting (Chambers et al. 2004), but it has also been implicated in verbally mediated fact retrieval during mathematical cognition tasks (Dehaene et al. 2004). However, resting-state functional magnetic resonance imaging (fMRI) and positron emission tomography studies have consistently identified the AG as a key parietal node of the default mode network (DMN) (Raichle et al. 2001; Greicius et al. 2003; Uddin et al. 2009), and task-related deactivations have been widely reported in the AG (Shulman et al. 1997; Wu et al. 2009).

Marking the dorsal border of the IPL is the infolding along the banks of the IPS, which separates the IPL from the superior parietal lobule and dorsally bounds the AG. Activation of the IPS has been reported during tasks involving visuo-spatial attention (Egner et al. 2008), visual short-term memory (Vogel et al. 2005; Xu and Chun 2009), basic number processing (Ansari and Dhital 2006; Nieder and Dehaene 2009), and numerical and ordered sequence processing (Cantlon et al. 2006; Ischebeck et al. 2007).

Recent cytoarchitectonic analyses of the human IPL have suggested that the AG and IPS can be parcellated into distinct subregions (Choi et al. 2006; Caspers et al. 2008). Using observer-independent definitions of cytoarchitectonic borders, Caspers and colleagues have defined 2 subdivisions within the AG, one anterior (PGa) and one posterior (PGp) (Caspers et al. 2006). Within the IPS, this group has demonstrated at least 3 cytoarchitectonically distinct areas, labeled hIP2, hIP1, and hIP3 (Caspers et al. 2008).

One way to gain insights into functional brain organization is by capitalizing on these methodological advances to examine functional and structural connectivity of putative distinct cortical regions. The study of large-scale brain networks offers novel insight into the integrated functioning of the human brain (Mesulam 1998). Connectivity analysis using resting-state fMRI data has become increasingly informative for understanding the role of specific brain regions from a systems neuroscience perspective. Studies of brain networks are shedding new light on

how different regions of the brain interact with each other during behavior and cognition. In particular, the existence of "intrinsic connectivity networks"—brain networks that are functionally coupled even in the absence of a task (Greicius et al. 2003; Seeley et al. 2007)—can provide novel insights into the integrative functions subserved by specific brain regions. Since the initial discovery of spontaneous low frequency correlations in blood oxygen level-dependent signal within the sensorimotor system at rest (Biswal et al. 1995), several other intrinsic connectivity networks have been described, including the DMN (Greicius et al. 2003; Fransson 2005), dorsal and ventral attention systems (Fox et al. 2006), and hippocampal memory systems (Vincent et al. 2006). Resting-state functional connectivity data have also been shown to differentiate brain networks in clinical populations (Castellanos et al. 2008; Kennedy and Courchesne 2008; Supekar et al. 2008; Seeley et al. 2009) and is related to cognition and behavior (Fox et al. 2007; Seeley et al. 2007; Kelly et al. 2008; Di Martino et al. 2009). Recently, resting-state fMRI has been used to describe distinct functional boundaries within the human IPL (Cohen et al. 2008).

In parallel to these advances in resting-state fMRI, recent refinements in the acquisition and analysis of diffusion tensor imaging (DTI) data have enabled the visualization of structural connections between discrete brain regions in vivo. DTI is a non-invasive imaging method that enables the study of white matter circuits in the human brain by examining directional diffusion of water restricted by the orientation and structure of axon bundles (Ben-Shachar et al. 2007; Hew et al. 2008; Jones 2008) and used alongside resting-state functional connectivity measures, can lead to a more complete characterization of human brain networks (Damoiseaux and Greicius 2009; Greicius et al. 2009). It has also recently been demonstrated that connectivity patterns obtained from DTI and resting-state fMRI data show significant agreement in many (Skudlarski et al. 2008; Honey et al. 2009; van den Heuvel et al. 2009), but not all cases (Uddin et al. 2008).

The recent availability of probabilistic cytoarchitectonic maps has the potential to inform and significantly enhance our understanding of the functional architecture of the human IPL. Cytoarchitectonic maps obtained from post-mortem brains suggest that the human IPL has a more finely grained parcellation than previously suggested by the classical Brodmann map (Caspers et al. 2008). Here, we examined the functional and structural connectivity of 2 anterior and posterior AG ROIs (PGa and PGp) and 3 hIP ROIs (hIP2, hIP1, and hIP3) encompassing 2 major subdivisions within the caudal and dorsal IPL. Using resting-state fMRI and DTI data collected from healthy adult participants, we mapped functional and structural networks associated with each of these ROIs and examined their differential patterns of whole-brain connectivity, taking note of differences in connectivity patterns within the AG and within the IPS. Our results demonstrate that these spatially adjacent and cytoarchitectonically distinct regions in the IPL have distinct patterns of long-range functional and structural connectivity.

Materials and Methods

Participants

All protocols were approved by the human participants Institutional Review Board at the Stanford University School of Medicine. All participants were volunteers and were treated in accordance with the American Psychological Association "Ethical Principles of Psychologists and Code of Conduct." Brain imaging data were obtained from 22 right-handed healthy adults (11 males and 11 females, mean age 20.24 ± 0.84). DTI data were obtained from 15 of 22 participants.

Data Acquisition

fMRI

Functional imaging data were acquired at the 3-T General Electric Signa Scanner at the Stanford Lucas Center using the following parameters: 2000 ms TR, 30 ms TE, 80° flip angle, and a 256 × 256 × 132 matrix using a spiral in, spiral in/out pulse sequence to reduce magnetic susceptibility artifacts (Li et al. 2006). A total of 29 axial slices (4.0 mm thickness, 0.5 mm skip) parallel to the AC-PC line and covering the whole brain were acquired. The field of view was 20 cm, and the matrix size was 64 × 64, providing an in-plane spatial resolution of 3.125 mm. Participants lay in the fMRI scanner with their eyes closed for the duration of an 8-minute resting-state scan. A high resolution T1-weighted spoiled grass gradient recalled inversion recovery 3D MRI sequence was acquired to facilitate anatomical localization of functional data using the following parameters: TI = 300 ms, TR = 8.4 ms; TE = 1.8 ms; flip angle = 15°; 22 cm field of view; 132 slices in coronal plane; 256 × 192 matrix; 2 NEX, acquired resolution = 1.5 × 0.9 × 1.1 mm.

DTI

The DTI pulse sequence was a diffusion-weighted single-shot spin-echo, echo planar imaging sequence (TE = 70.8 ms; TR = 8.6 s; field of view = 220 mm; matrix size = 128 × 128; bandwidth = ±110kHz; partial k-space acquisition). We acquired 63 axial, 2-mm thick slices (no skip) for 2 *b* values, $b = 0$ and b = approximately 850 s/mm^2. The high *b* value was obtained by applying gradients along 23 different diffusion directions. Two gradient axes were energized simultaneously to minimize TE. The polarity of the effective diffusion-weighting gradients was reversed for odd repetitions to reduce cross-terms between diffusion gradients and imaging and background gradients. Although it has been suggested that measuring more diffusion directions is a more efficient way to reliably estimate diffusion tensors of arbitrary orientation (Jones 2004), our signal-to-noise ratio is sufficiently high from our 4 repeats to produce very reliable tensor estimates suitable for tractography (Mori 2007; Sherbondy et al. 2008).

fMRI Data Preprocessing

Data were preprocessed using SPM5. Images were corrected for movement using least-square minimization without higher order corrections for spin history (Friston et al. 1995) and normalized to the Montreal Neurologic Institute template. Resulting images were then resampled every 2 mm via sinc interpolation and smoothed with a 6-mm Gaussian kernel to reduce spatial noise. High and low frequency artifacts were removed through the implementation of a bandpass filter (0.00833 to 0.15 Hz) on the smoothed data.

Regions-of-Interest

Five source region-of-interest (ROI) masks in each hemisphere were constructed using maximum probability maps (MPMs) defined through the Anatomy Toolbox in SPM5. These MPMs allow the definition of non-overlapping regions from cytoarchitectonic probability maps that are inherently overlapping (Eickhoff et al. 2005; Caspers et al. 2008). ROIs derived from these maps using the MarsBar tool (http://marsbar.sourceforge.net/) consisted of the left and right anterior AG (PGa), posterior AG (PGp, Fig. 1*a*) and IPS (hIP2, hIP1, and hIP3, Fig. 2*a*). Detailed information about the anatomical boundaries of these maps has been published elsewhere (Caspers et al. 2006; Choi et al. 2006; Caspers et al. 2008). These 10 ROIs were used as seeds in a resting-state functional connectivity analysis, as well as starting points in deterministic tractography analyses as described below.

Resting-State Functional Connectivity Analysis

Functional connectivity of each left and right region's source ROI was computed individually using methods similar to those described in (Etkin et al. 2009; Habas et al. 2009). For each ROI, a seed resting-state time series was extracted by averaging the time series of all voxels within it. The resulting ROI time series was then used as a covariate of interest

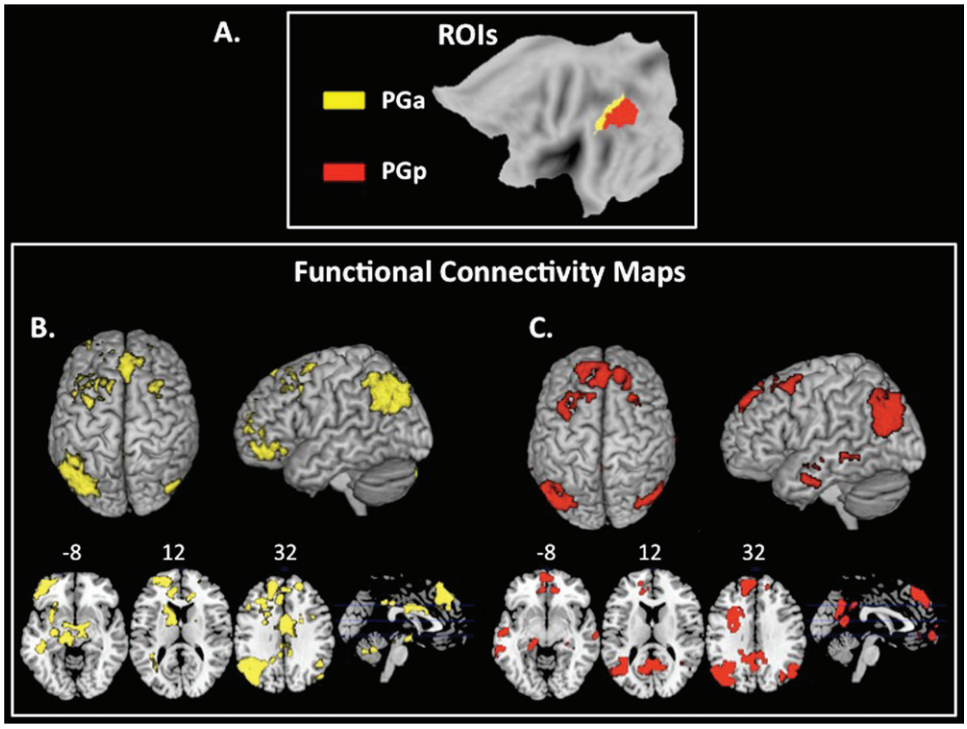

Figure 1. Functional connectivity of PG subdivisions. (*a*) ROIs derived from cytoarchitectonic maps for PGa (yellow) and PGp (red). (*b*) Functional connectivity map associated with anterior AG (PGa) source ROI in the left hemisphere. The color yellow represents voxels correlated with the source ROI, colored to match the ROI itself. Group-level maps were thresholded at $P < 0.001$ FWE, cluster threshold of 100 voxels. (*c*) Functional connectivity map associated with posterior AG (PGp) source ROI in the left hemisphere. The color red represents voxels correlated with the source ROI, colored to match the ROI itself. Group-level maps were thresholded at $P < 0.001$ FWE, cluster threshold of 100 voxels.

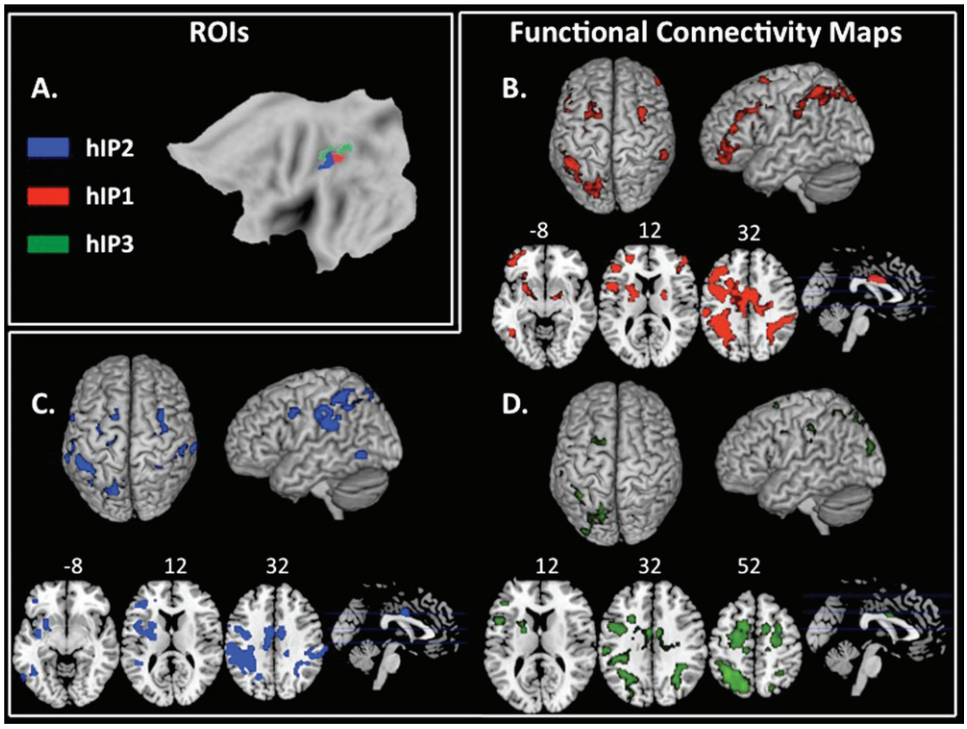

Figure 2. Functional connectivity of hIP subdivisions. (*a*) ROIs derived from cytoarchitectonic maps for hIP1 (red), hIP2 (blue), and hIP3 (green). (*b*) Functional connectivity map associated with hIP1 source ROI in the left hemisphere. The color red represents voxels correlated with the source ROI, colored to match the ROI itself. Group-level maps were thresholded at $P < 0.001$ FWE, cluster threshold of 100 voxels. (*c*) Functional connectivity map associated with hIP2 source ROI in the left hemisphere. The color blue represents voxels correlated with the source ROI, colored to match the ROI itself. Group-level maps were thresholded at $P < 0.001$ FWE, cluster threshold of 100 voxels. d. Functional connectivity map associated with hIP3 source ROI in the left hemisphere. The color green represents voxels correlated with the source ROI, colored to match the ROI itself. Group-level maps were thresholded at $P < 0.001$ FWE, cluster threshold of 100 voxels.

in a linear regression whole-brain analysis. A global time series, computed across all brain voxels, along with 6 motion parameters, were used as additional covariates to remove confounding effects of physiological noise and participant movement. Ten separate linear regressions were conducted at the individual subject level, each using a different ROI time series from one of the 10 source ROIs as a covariate of interest. Group-level functional connectivity maps of each ROI were then generated using one-sample *t*-tests of individual functional connectivity contrast images. Group level functional connectivity maps were stringently thresholded using family-wise error (FWE) correction at the whole-brain level ($P < 0.001$ FWE, cluster threshold of 100 voxels) to reveal regions most robustly correlated with each ROI.

Direct comparisons between target maps of multiple source ROIs were computed using ANOVAs with false discovery rate (FDR) corrections at the whole-brain level ($P < 0.05$ FDR, and $P < 0.05$ FWE correction at the cluster level). To limit problems with multiple comparisons, we restricted the analysis to 2 separate whole-brain ANOVAs. The first ANOVA assessed differences between the 2 AG (PGa and PGp) connectivity maps using *t*-contrasts (PGa > PGp and PGp > PGa); the second assessed differences between the 3 IPS (hIP2, hIP1, and hIP3) connectivity maps using *t*-contrasts (hIP1 > [hIP2 and hIP3] and hIP3 > [hIP1 and hIP2]). For these ANOVAs, results were masked by the combined functional connectivity maps of the source ROIs (combined maps of PGa and PGp for the first ANOVA and combined maps of hIP2, hIP1, and hIP3 for the second ANOVA).

To illustrate differential connectivity of each source ROI to specific target brain regions, contrast maps from the ANOVA were masked with target regions selected from the Anatomical Automatic Labeling (AAL) atlas within the MarsBar SPM Toolbox (Fig. S1, Table 1), and 3-mm spheres around peak voxels were created (Table 2). *T*-scores of functional connectivity strength between each source ROI (PGa, PGp, hIP2, hIP1, and hIP3) and their targets were plotted (Fig. 3*b,d* and Fig. 4*b,d*).

DTI Analyses

DTI data were preprocessed to remove eddy current distortion effects and determine a constrained nonrigid image registration of the diffusion images, using an algorithm based on normalized mutual information (Bammer et al. 2002). Multivariate regression was used to determine the 6 elements of the diffusion tensor (Basser 1995; Basser and Pierpaoli 1996). For each participant, the non-diffusion-weighted (B0) images were coregistered to the T1-weighted anatomical images using SPM's 3-D rigid-body coregistration algorithm. Coregistration of DTI and T1 images was confirmed by visual inspection of each dataset to ensure alignment. Anatomical landmarks including the anterior commissure, posterior commissure, and midsagittal plane were identified by hand on the anatomical images and used to compute a rigid-body transform from the native image space to the conventional AC-PC aligned space. DTI data were resampled to this AC-PC aligned space with 2-mm isotropic voxels using a spline-based tensor interpolation algorithm (Pajevic et al. 2002). The tensors were rotated to the same space using algorithms designed to preserve their orientation with respect to brain anatomy (Stuss et al. 2001). Anatomical images were resampled to AC-PC-aligned space with 1-mm isotropic voxels. Coregistration of DTI and T1 images was confirmed by visual inspection of each dataset to ensure alignment. Fiber tractography was used to estimate likely structural connections. Custom DTI analysis software (http://sirl.stanford.edu/software/) was used to initiate whole-brain fiber tracking. We were specifically interested in looking for tracts between the source ROIs and target structures determined from examination of the resting-state functional connectivity analyses. Target structures were ROIs obtained from the AAL atlas within the MarsBar SPM Toolbox. Specifically, we searched for fiber tracts between pairs of structures initially identified using the functional connectivity analyses, as described above (Fig. S1, Table 1). The source (PGa, PGp, hIP2, hIP1, and hIP3) and target AAL ROIs were then warped back to each individual brain by applying the inverse of the spatial normalization transformation so that they could be used for the subsequent DTI tractography analyses. As fiber tracking becomes unreliable in gray matter, we ensured that our ROIs extended 3–4 mm into the white matter. Tracts that did not end in or pass through both source and target ROIs were discarded. Each fiber tract was estimated using a deterministic streamlined tracking algorithm with a fourth order Runge–Kutta path integration method and 1 mm fixed step size (Mori et al. 1999; Barton et al. 2002). A continuous tensor field was estimated using trilinear interpolation of the tensor elements. Starting from the initial seed point, fiber paths were traced in both directions along the principal diffusion axis. Path tracing proceeded until the fractional anisotropy (FA) fell below 0.15 or until the minimum angle between the current and previous path segments was larger than 30°. To limit the number of false positives, fibers that were anatomically implausible were identified visually and removed. It should be noted that a limitation of all current DTI work is that tractography results are susceptible to the confound of crossing fibers, which potentially may lead to both false positives and false negatives in structural connectivity analyses. However, the majority of known false negatives in tractography studies involve small laterally running tracts that are lost when crossing larger tracts like the longitudinal fasiculii and corona radiata (Dougherty et al. 2005). In our study, we did not examine such small tracts precisely because of this concern. It is also the case that tractography results may produce false positives. However, their likelihood is relatively low with the stringent tractography parameters used in our analysis.

DTI Measures of Structural Connectivity

For each subject, the density of the fibers connecting each source to target ROI pair was measured. The density of fibers connecting 2 regions u and v was computed as:

$$\text{fiber-density}(\mathrm{u},\mathrm{v}) = \frac{2}{Su + Sv}\sum_{f \in F(u,v)} \frac{1}{l(f)} \qquad (1)$$

where F(u,v) is a set of all the fibers f connecting u and v, l(f) is the length of the individual fiber, Su and Sv are sizes of the ROIs (eq. 1, Hagmann et al. 2008). The fiber density (number of fibers per unit surface), a measure of structural connectivity, approximates the axonal number interconnecting the ROIs. Fiber density has been used previously to quantify structural connectivity, particularly to measure the integrity of white matter (Hagmann et al. 2008; van den Heuvel et al. 2008). In our study, we used fiber density as a measure of the integrity of the fiber tracts connecting ROIs. Fractional anisotropy (FA) values for each of the ROI pairs are reported in Supplementary Materials (Table S1). To interpret the anatomical location of the DTI tracts, we referenced the Johns Hopkins University-International Consortium for Brain Mapping white matter atlas and labeled our results by visual inspection.

Table 1

Source (cytoarchitectonic) and target (AAL atlas) ROIs for functional and structural connectivity analyses. See Figures 1*a* and 2*a*, and Figure S1

Source cytoarchitectonic ROIs	Target AAL ROIs
PGa	Caudate
PGp	Putamen
	Hippocampus
	Parahippocampal gyrus
hIP2	Inferior frontal opercular
hIP1	Inferior frontal triangular
hIP3	Insula
	Superior occipital

Table 2

Coordinates of peak signal within each AAL ROI from functional connectivity analysis of PGa, PGp, hIP2, hIP1, and hIP3. See Figures 3 and 4

Functional connectivity contrast	Masked with target AAL ROI	Peak coordinate
PGa > PGp	Caudate	−8 2 14
PGp > PGa	Hippocampus	−26 −20 −20
PGp > PGa	Parahippocampal	−26 −22 −22
hIP1 > hIP2, hIP3	Inferior frontal opercular	−44 20 34
hIP1 > hIP2, hIP3	Inferior frontal triangular	−38 44 2
hIP1 > hIP2, hIP3	Insula	−28 18 −4
hIP3 > hIP1, hIP2	Superior occipital	−14 −100 16

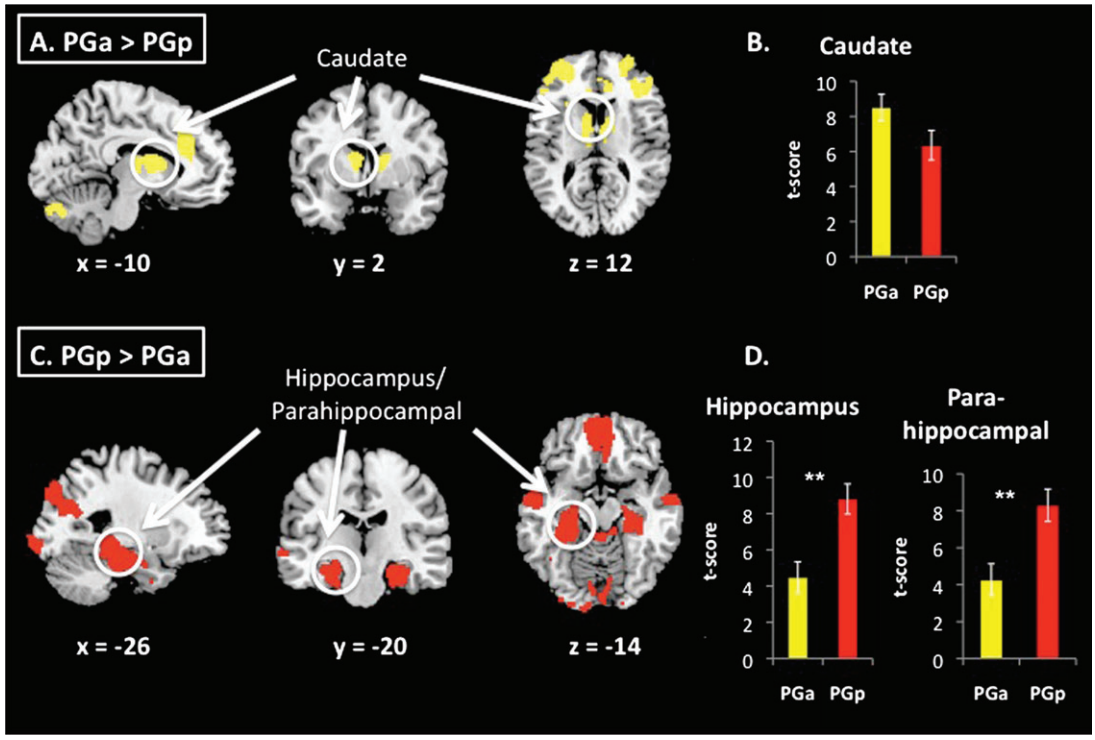

Figure 3. Comparison of functional connectivity between PG subdivisions. (*a*,*c*) Direct contrasts of functional connectivity maps associated with PGa and PGp ROIs, from ANOVA (FDR corrections at the whole brain level [$P < 0.05$ FDR and $P < 0.05$ FWE correction at the cluster level]). PGa was more strongly correlated with caudate, whereas PGp was more strongly correlated with hippocampus. (*b*,*d*) Bar graphs show *t*-scores within peak coordinates where the contrast maps overlapped with target ROIs ($*P < 0.05$, $**P < 0.01$).

Results

Functional Connectivity: PGa and PGp

The left PGa showed functional connectivity with the homologous area in the right hemisphere (AG) and with posterior, and mid- and anterior cingulate, bilateral superior frontal gyrus, bilateral frontal pole, left middle and inferior frontal gyrus, left anterior insula, left caudate, and left posterior middle and inferior temporal gyrus (Fig. 1*b*).

The left PGp was correlated with the right AG and adjacent lateral occipital cortex, the precuneus and posterior cingulate, bilateral middle temporal gyrus, bilateral parahippocampal and hippocampal gyri, left middle and inferior frontal gyrus, bilateral superior frontal gyrus, bilateral frontal pole, and ventromedial frontal cortex (Fig. 1*c*, Table S2).

Direct comparisons of the PGa and PGp revealed greater connectivity of left PGa with caudate, bilateral frontal poles, and posterior and anterior cingulate (Fig. 3*a*). PGp showed greater connectivity than PGa with medial prefrontal cortex, hippocampus and parahippocampal gyrus, and precuneus and the occipital poles (Fig. 3*c*, Table S3). Average *t*-scores showing differential connectivity of PGa and PGp to target structures are plotted in Figure 3*b*,*d*.

Right hemisphere ROIs showed a similar, although weaker, pattern of connectivity as left hemisphere ROIs (Figs S2 and S3).

Structural Connectivity: PGa and PGp

Fiber densities were computed between each of the source ROIs (PGa and PGp) and target AAL ROIs identified from functional connectivity analyses (Fig. S1). PGp showed greater density of fibers connecting to the hippocampus and parahippocampal ROIs than did PGa (Fig. 5*a*). These fibers primarily overlap with the inferior longitudinal fasciculus. In contrast, both the PGa and PGp showed fiber tracts to the caudate via the inferior fronto-occipital fasciculus. However, there were no significant differences between density of fibers connecting PGa and PGp to the target caudate ROI (Fig. 5*b*).

Functional Connectivity: hIP2, hIP1, and hIP3

The left hIP2 showed strong functional connectivity with the right supramarginal gyrus, left inferior frontal gyrus extending ventrally into the insular cortex, left posterior middle temporal gyrus, bilateral precentral gyrus extending rostrally to superior frontal gyrus, mid-cingulate, left putamen, and left frontal pole (Fig. 2*c*).

Left hIP1 was correlated with bilateral lateral occipital cortex extending rostrally through the angular and supramarginal gyri, mid-cingulate, bilateral precentral gyri, left inferior and middle frontal gyri and frontal pole, left inferior temporal gyrus, left insula, and left putamen (Fig. 2*b*).

Left hIP3 was correlated with bilateral superior lateral occipital cortex extending into supramarginal gyrus, bilateral superior frontal gyri, left precentral gyrus, and left inferior frontal gyrus (Fig. 2*d*, Table S2).

Direct comparisons of hIP2, hIP1, and hIP3 in an ANOVA revealed greater connectivity of hIP1 compared with hIP2 and hIP3 with a large cluster extending from bilateral angular gyri to the frontal pole (Fig. 4*a*). Closer examination of this difference by plotting *t*-scores showed that the difference was driven by hIP1 > hIP2 in the opercular region of the inferior frontal cortex and hIP1 > hIP3 in the triangular region of the inferior frontal cortex (Fig. 4*b*).

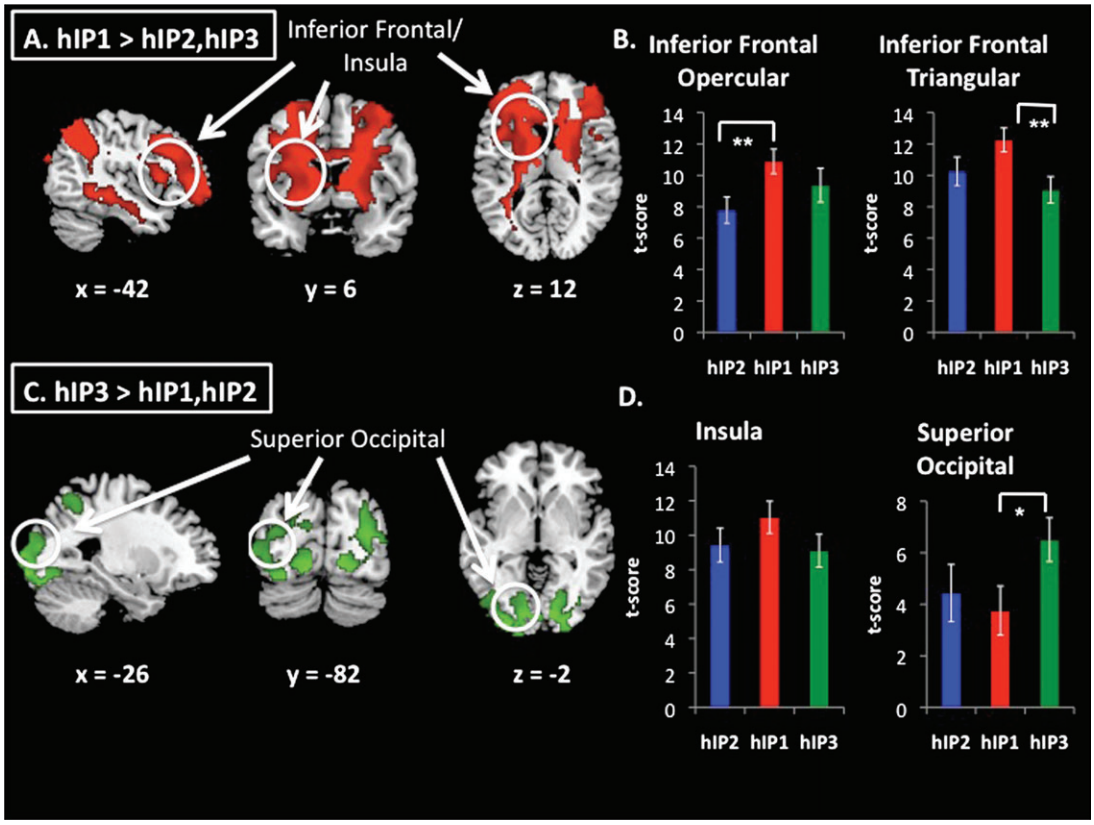

Figure 4. Comparison of functional connectivity between hIP subdivisions. (*a*,*c*). Direct contrasts of functional connectivity maps associated with hIP2, hIP1, and hIP3 ROIs, from ANOVA (FDR corrections at the whole brain level [$P < 0.05$ FDR and $P < 0.05$ FWE correction at the cluster level]). hIP1 was more strongly correlated with inferior frontal cortex and insula, whereas hIP3 was more strongly correlated with superior occipital cortex. (*b*,*d*) Bar graphs show *t*-scores within peak coordinates where the contrast maps overlapped with target ROIs ($*P < 0.05$, $**P < 0.01$). Signal differences in the opercular regions of the inferior frontal cortex were mainly driven by hIP1 > hIP2, whereas signal differences in the triangular regions of the inferior frontal cortex were mainly driven by hIP1 > hIP3. Signal differences in superior occipital cortex were mainly driven by hIP3 > hIP1.

hIP3 showed greater connectivity than hIP1 and hIP2 with bilateral occipital poles and adjacent cortices (Fig. 2*b*, Table S3). Average *t*-scores showing differential connectivity of hIP3, hIP2, and hIP1 to occipital areas are shown in Figure 4*d*. The hIP3 connectivity differences were mainly driven by hIP3 > hIP1 in superior occipital cortex.

Structural Connectivity: hIP2, hIP1, and hIP3

Fiber densities were computed between each of the source ROIs (hIP2, hIP1, and hIP3) and targets identified from functional connectivity analyses (Fig. S1, Table 1). Both hIP2 and hIP1 showed greater density of fibers along the superior longitudinal fasciculus connecting to the ROI in the opercular region of the inferior frontal cortex (Fig. 6*a*) than did hIP3. hIP1 showed greater density of fibers than both hIP2 and hIP3 along the superior longitudinal fasciculus connecting to the insula (Fig. 6*b*). hIP3 showed greater density of fibers along the inferior fronto-occipital fasciculus connecting to the superior occipital ROI than did hIP2 (Fig. 6*c*).

Discussion

The human IPL participates in a wide array of cognitive functions, but critical distinctions between subdivisions within this region have not been systematically explored. We separately mapped the resting-state functional connectivity and structural connectivity of 2 major subdivisions of the IPL. We examined IPL connectivity of cytoarchitectonically defined regions encompassing the anterior and posterior AG subregions PGa and PGp and 3 IPS subregions hIP2, hIP1, and hIP3 (Caspers et al. 2006). We examined resting-state functional connectivity using fMRI and structural connectivity using DTI. Qualitatively, the AG and IPS regions overall exhibited differential patterns of functional and structural connectivity. The AG was unique in its connectivity with structures classically regarded as integral to the brain's core memory systems, including the medial temporal lobe and the basal ganglia (Squire 2009), whereas IPS showed unique patterns of connectivity to frontal and occipital lobe structures. Both functional and structural connectivity analyses revealed differential coupling between different subregions of the IPL, allowing us to demonstrate the unique functional architecture of each IPL division. Our findings suggest that cytoarchitectonically distinct subdivisions of the human IPL have different patterns of cortical and subcortical connectivity and provide new insights into the functional organization of the PPC. We discuss findings from connectivity analyses of the 2 major subdivisions—AG and IPS—and their implications for a more principled interpretation of functional neuroimaging studies reporting activations and deactivations within the parietal cortex.

AG: PGa/PGp

The PGa and PGp ROIs, while adjacent, showed striking differences with respect to resting-state functional connectivity and white matter tractography. The PGp ROI showed

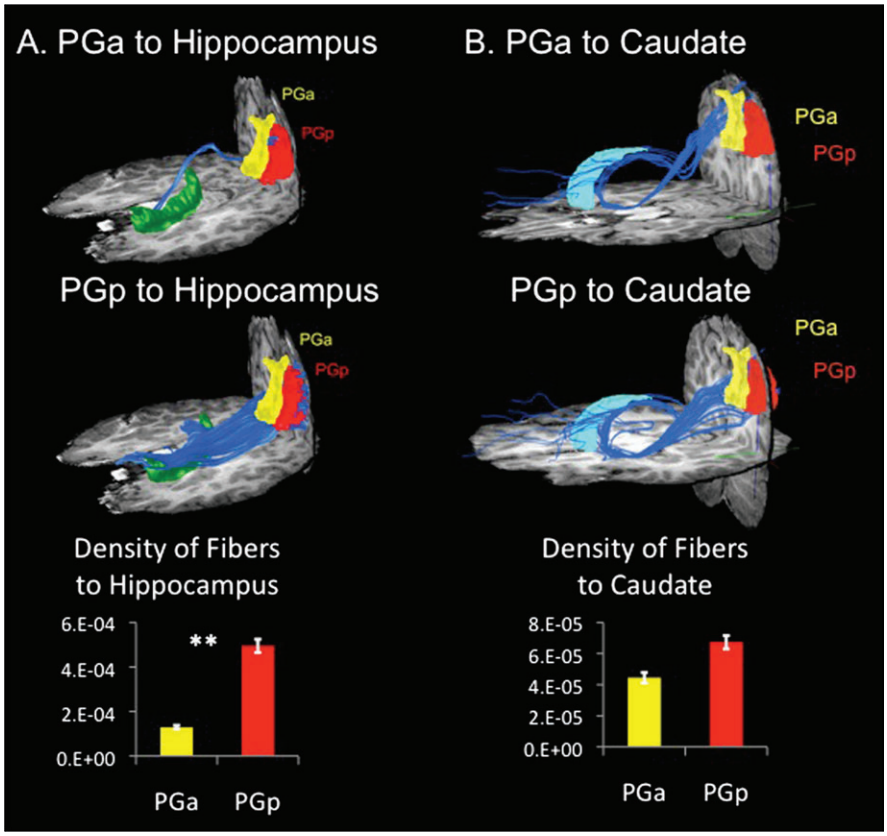

Figure 5. Structural connectivity of PG subdivisions. (*a*) DTI tractography and density of fibers between PGa and PGp and target AAL ROI hippocampus. PGp showed greater structural connectivity with hippocampus than did PGa (**$P < 0.01$). (*b*) DTI tractography and density of fibers between PGa and PGp and target AAL ROI caudate. PGa and PGp did not differ significantly in structural connectivity with caudate.

significantly stronger functional connectivity with regions belonging to the DMN, including medial prefrontal cortex, posterior cingulate, and precuneus (Raichle et al. 2001). Additionally, PGp showed stronger functional connectivity than PGa with hippocampal and parahippocampal regions, also considered part of the DMN (Greicius et al. 2003; Greicius et al. 2004). Structural connectivity, reflected in the density of fibers, was likewise strong between PGp and hippocampus/parahippocampus, a finding consistent with previous probabilistic tractography work (Rushworth et al. 2006). Our study shows that PGp has much stronger functional and structural connectivity via the inferior longitudinal fasciculus. While there is a growing body of literature examining the cortical midline structures comprising the DMN (van den Heuvel et al. 2008; Uddin et al. 2009), the lateral parietal nodes have not been previously well delineated. Here, we show for the first time that the more posterior subdivision of the AG (PGp) is more closely associated with the entire DMN than the adjacent anterior AG (PGa).

The fact that the AG can be subdivided into regions with distinct connectivity patterns helps to address a problem in functional neuroimaging literature with respect to interpreting changes in activation levels against baseline. Previous studies reporting increased activation of the AG did not distinguish between anterior and posterior AG engagement during arithmetic fact retrieval and computation (Ischebeck et al. 2009). A recent study demonstrated that the PGp is more deactivated during a mental arithmetic task than the PGa (Wu et al. 2009). However, it is unclear whether this was a result of differences in functional and structural circuitry associated with PGa and PGp, as opposed to differences in baseline. The distinct patterns of PGa and PGp connectivity shown here critically inform our understanding of the manner in which specific areas of the AG are consistently engaged or disengaged during mathematical cognition.

The PPC is known to be critically involved in both spatial and non-spatial attention (Coull et al. 2004; Shulman et al. 2009). Current models of attention make a distinction between 2 frontoparietal attention networks, one dorsal ("top-down" attention) and one ventral ("bottom-up" attention) (Corbetta and Shulman 2002; Sridharan et al. 2007). In a recently developed model, Cabeza and colleagues propose that the distinction between dorsal and ventral attention systems can explain parietal contributions to episodic memory. According to the attention to memory (AtoM) model, the dorsal parietal system is involved with the allocation of resources to memory retrieval (top-down), while the ventral parietal system is associated with the capture of attentional resources by relevant memory cues (bottom-up) (Cabeza et al. 2008). The ventral attention system is comprised of a somewhat anatomically ill-defined region known as the temporo-parietal junction and the ventrolateral prefrontal cortex. Because of the lack of unambiguous gyral and sulcal landmarks, the AG has been considered to be part of the ventral frontoparietal attention system (Chambers et al. 2004). Our functional connectivity results demonstrate strong coupling specifically between PGa

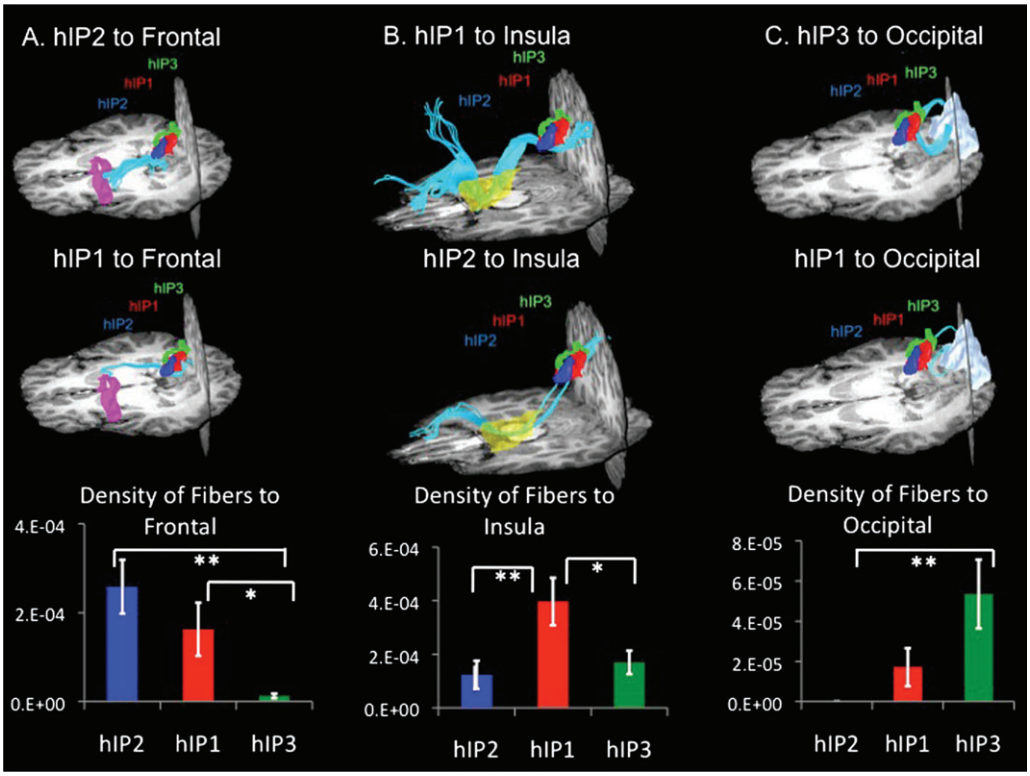

Figure 6. Structural connectivity of hIP subdivisions. (*a*) DTI tractography and density of fibers between hIP2, hIP1 and hIP3 and target AAL ROI inferior frontal opercular. Both hIP2 and hIP1 showed greater structural connectivity with inferior frontal opercular than did hIP3 ($*P < 0.05$, $**P < 0.01$). (*b*) DTI tractography and density of fibers between hIP2, hIP1, and hIP3 and target AAL ROI insula. hIP1 showed greater structural connectivity than hIP2 and hIP3 with insula ($*P < 0.05$, $**P < 0.01$). (*c*) DTI tractography and density of fibers between hIP2, hIP1, and hIP3 and target AAL ROI superior occipital cortex. hIP3 showed greater structural connectivity with superior occipital cortex than did hIP2 ($**P < 0.01$).

and ventrolateral prefrontal cortex, suggesting that this AG subdivision can be considered as more closely associated with the ventral attention system than the PGp.

The neural substrates of spatial working memory processes overlap to a large degree with those areas involved in spatial attention (Awh and Jonides 2001). It has previously been shown that basal ganglia and prefrontal cortex activity precedes the filtering of irrelevant information and that this activity is a significant predictor of working memory capacity (McNab and Klingberg 2008). Our analyses revealed greater coupling of the PGa with basal ganglia, suggesting a pathway through which this proposed attentional control over access to working memory storage in the parietal cortex could occur. Previous resting-state fMRI study also demonstrated functional connectivity between the caudate and IPL (Di Martino et al. 2008; Shulman et al. 2009), as we report here.

While much of the literature on attention and memory processes focuses on fronto-parietal networks, the precise parietal regions involved are often poorly specified. Our analyses suggest that a greater degree of anatomical specificity is critical to understanding parietal contributions to these cognitive processes, as different parietal subdivisions preferentially interact with different large-scale brain networks.

A recent meta-analysis of 120 functional neuroimaging language studies of semantic processing identifies the left AG as the region showing the most dense concentration of activation foci involved in the semantic system of the human brain (Binder et al. 2009). As the authors noted, the region of the AG is greatly expanded in the human brain compared with non-human primates, potentially providing a neural substrate for the capacity for language to develop. Our analysis links the PGa more closely with anterior language regions in the inferior frontal gyrus than the PGp, providing a more precise delineation of parietal contributions to language networks.

IPS: hIP2, hIP1, and hIP3

Despite their close proximity along the IPS, the 3 hIP ROIs exhibit functional connectivity to different neural networks. The differences in functional connectivity of these neighboring regions reflect the multimodal nature of the IPS, which acts as a convergence zone integrating multiple cognitive functions. The IPS region, along with the frontal eye fields, has been described as belonging to the dorsal attention system for top-down attentional orienting (Corbetta and Shulman 2002). However, previous neuroimaging studies in the human brain have not taken into account potential heterogeneity within subdivisions of the IPS. Our functional connectivity analyses show strong coupling between the anterior IPS ROIs (hIP2 and hIP1) and frontal attentional regions. In sharp contrast, the posterior IPS region (hIP3) shows strong coupling with posterior occipital regions. This distinction is consistent with macaque anatomical studies, which have shown strong connections between the anterior IPS (AIP) and ventral premotor cortex and the posterior IPS (CIP) to visual cortices (Grefkes and Fink 2005). One previous DTI study reported structural connectivity between the anterior IPS and ventral premotor cortex (Rushworth et al. 2006), consistent with our results. Our study extends previous findings by showing

convergence with functional connectivity and cytoarchitectonic mapping of the human IPS.

Beyond spatial attention, one of the cognitive domains most consistently associated with the IPS is numerical cognition. This region is thought to facilitate amodal, language-independent, semantic representations of numerical quantity (Dehaene et al. 2004; Rosenberg-Lee et al. 2009). In healthy adults, the IPS is modulated by the complexity of numerical (Baron-Cohen et al. 2000; Duffau et al. 2002; Delazer et al. 2003; Ansari et al. 2006; Castelli et al. 2006; Cohen Kadosh et al. 2007; Piazza et al. 2007) and arithmetic (Burbaud et al. 1995; Dehaene et al. 1999; Menon et al. 2000; Gruber et al. 2001) reasoning. Neuroimaging studies of dyscalculia (a deficit specifically in the numerical domain) have also revealed abnormalities of the IPS, including reduced gray matter (Isaacs et al. 2001; Rotzer et al. 2008), abnormal sulcal depth (Molko et al. 2003), and hypoactivation of the region (Kesler et al. 2006; Price et al. 2007) in individuals with mathematical difficulties. Our results suggest that the anterior and posterior IPS subdivisions play different roles in processing numerical information. The posterior IPS (hIP3), by virtue of its greater functional and structural connectivity with visual cortex, may play a leading role in transforming symbolic and non-symbolic numerical information to spatial and semantic representations of quantity. In contrast, the more anterior IPS regions (hIP2 and hIP1) may support more complex aspects of numerical and mathematical information processing via their interconnections with fronto-parietal circuits. Our tractography findings suggest that fibers along the superior longitudinal fasciculus play a major role in this interaction.

In both the human and macaque brain, the anterior IPS coordinates visuomotor actions such as reaching, grasping, and eye movements (Frey et al. 2005; Culham and Valyear 2006). In contrast, the posterior-most IPS region has been shown to participate in peripersonal visual representations (Makin et al. 2007). Damage to the occipitotemporal visual system (ventral visual stream) in the presence of an intact occipitoparietal system (dorsal visual stream) (Goodale and Milner 1992) can result in spared visuomotor skills in the presence of severe visual form agnosia (James et al. 2003), as demonstrated most dramatically by a patient studied by Goodale and Milner (Goodale and Milner 1992). Importantly, we found that hIP2 and hIP1, the anterior-most IPS subdivision, showed strong functional and structural connectivity with the premotor cortex and the inferior frontal gyrus. Our connectivity analyses of networks associated with the IPS suggest a general principle of organization whereby posterior IPS regions that are closely linked to the visual system transform stimuli into motor action through the anterior IPS connections to the prefrontal cortex.

Our functional and structural connectivity results point to strong connections between hIP1 and insula. Anatomical tracer studies in the macaque have shown connections between posterior insula and parietal area PF (Mesulam and Mufson 1982). The current results demonstrate IPS–insula structural connectivity for the first time in humans. We suggest that this inter-connected system may help to mediate detection of visually salient stimuli.

Conclusion

The caudal and dorsal IPL can be divided into 5 major subdivisions based on cytoarchitectonic features (Caspers et al. 2008). We have shown that the AG and IPS subdivisions of the IPL are associated with overlapping yet distinct functional and structural networks. The multiple dissociable networks associated with specific IPL cytoarchitectonic subdivisions facilitate contrasting, yet integrative cognitive functions in the human brain. The patterns of connectivity identified here provide links between anatomy and connectivity and facilitate more principled interpretation of diverse functional neuroimaging studies reporting activations and deactivations within this heterogeneous parietal region. More broadly, our findings provide new information about the functional and structural organization of the human parietal cortex and provide a novel synthesis of task-related activations and deactivations reported during different cognitive tasks.

Supplementary Material

Supplementary material can be found at: http://www.cercor.oxfordjournals.org/.

Funding

Children's Health Research Program, Lucille Packard Children's Hospital to L.Q.U.; National Institutes of Health (NS048302 to M.D.G., NS058899, HD047520, HD059205, HD057610 to V.M.); National Science Foundation (BCS/DRL 0449927) to V.M.

Notes

The authors gratefully acknowledge Dr. Simon Eickhoff and his colleagues at Jena for providing the research community with cytoarchitectonic maps of the human parietal cortex, Jose Anguiano for assistance with data acquisition, Katie Keller for assistance with data analysis, and Maria Barth for assistance with DTI figure construction. Tashia and John Morgridge endowed Postdoctoral Fellow at Lucille Packard Children's Hospital. *Conflict of Interest*: None declared.

References

Ansari D, Dhital B. 2006. Age-related changes in the activation of the intraparietal sulcus during nonsymbolic magnitude processing: an event-related functional magnetic resonance imaging study. J Cogn Neurosci. 18:1820–1828.

Ansari D, Dhital B, Siong SC. 2006. Parametric effects of numerical distance on the intraparietal sulcus during passive viewing of rapid numerosity changes. Brain Res. 1067:181–188.

Awh E, Jonides J. 2001. Overlapping mechanisms of attention and spatial working memory. Trends Cogn Sci. 5:119–126.

Bammer R, Auer M, Keeling SL, Augustin M, Stables LA, Prokesch RW, Stollberger R, Moseley ME, Fazekas F. 2002. Diffusion tensor imaging using single-shot SENSE-EPI. Magn Reson Med. 48:128–136.

Baron-Cohen S, Ring HA, Bullmore ET, Wheelwright S, Ashwin C, Williams SC. 2000. The amygdala theory of autism. Neurosci Biobehav Rev. 24:355–364.

Barton JJ, Press DZ, Keenan JP, O'Connor M. 2002. Lesions of the fusiform face area impair perception of facial configuration in prosopagnosia. Neurology. 58:71–78.

Basser PJ. 1995. Inferring microstructural features and the physiological state of tissues from diffusion-weighted images. NMR Biomed. 8:333–344.

Basser PJ, Pierpaoli C. 1996. Microstructural and physiological features of tissues elucidated by quantitative-diffusion-tensor MRI. J Magn Reson B. 111:209–219.

Ben-Shachar M, Dougherty RF, Wandell BA. 2007. White matter pathways in reading. Curr Opin Neurobiol. 17:258–270.

Binder JR, Desai RH, Graves WW, Conant LL. 2009. Where is the semantic system? A critical review and meta-analysis of 120 functional neuroimaging studies. Cereb Cortex. 19:2767–2796.

Biswal B, Yetkin FZ, Haughton VM, Hyde JS. 1995. Functional connectivity in the motor cortex of resting human brain using echo-planar MRI. Magn Reson Med. 34:537–541.

Brownsett SL, Wise RJ. forthcoming 2009. The contribution of the parietal lobes to speaking and writing. Cereb Cortex.
Burbaud P, Degreze P, Lafon P, Franconi JM, Bouligand B, Bioulac B, Caille JM, Allard M. 1995. Lateralization of prefrontal activation during internal mental calculation: a functional magnetic resonance imaging study. J Neurophysiol. 74:2194–2200.
Cabeza R, Ciaramelli E, Olson IR, Moscovitch M. 2008. The parietal cortex and episodic memory: an attentional account. Nat Rev Neurosci. 9:613–625.
Cantlon JF, Brannon EM, Carter EJ, Pelphrey KA. 2006. Functional imaging of numerical processing in adults and 4-y-old children. PLoS Biol. 4:e125.
Caspers S, Eickhoff SB, Geyer S, Scheperjans F, Mohlberg H, Zilles K, Amunts K. 2008. The human inferior parietal lobule in stereotaxic space. Brain Struct Funct. 212:481–495.
Caspers S, Geyer S, Schleicher A, Mohlberg H, Amunts K, Zilles K. 2006. The human inferior parietal cortex: cytoarchitectonic parcellation and interindividual variability. Neuroimage. 33:430–448.
Castellanos FX, Margulies DS, Kelly C, Uddin LQ, Ghaffari M, Kirsch A, Shaw D, Shehzad Z, Di Martino A, Biswal B, et al. 2008. Cingulate-precuneus interactions: a new locus of dysfunction in adult attention-deficit/hyperactivity disorder. Biol Psychiatry. 63:332–337.
Castelli F, Glaser DE, Butterworth B. 2006. Discrete and analogue quantity processing in the parietal lobe: a functional MRI study. Proc Natl Acad Sci USA. 103:4693–4698.
Chambers CD, Payne JM, Stokes MG, Mattingley JB. 2004. Fast and slow parietal pathways mediate spatial attention. Nat Neurosci. 7:217–218.
Choi HJ, Zilles K, Mohlberg H, Schleicher A, Fink GR, Armstrong E, Amunts K. 2006. Cytoarchitectonic identification and probabilistic mapping of two distinct areas within the anterior ventral bank of the human intraparietal sulcus. J Comp Neurol. 495:53–69.
Cohen AL, Fair DA, Dosenbach NU, Miezin FM, Dierker D, Van Essen DC, Schlaggar BL, Petersen SE. 2008. Defining functional areas in individual human brains using resting functional connectivity MRI. Neuroimage. 41:45–57.
Cohen Kadosh R, Cohen Kadosh K, Linden DE, Gevers W, Berger A, Henik A. 2007. The brain locus of interaction between number and size: a combined functional magnetic resonance imaging and event-related potential study. J Cogn Neurosci. 19:957–970.
Corbetta M, Shulman GL. 2002. Control of goal-directed and stimulus-driven attention in the brain. Nat Rev Neurosci. 3:201–215.
Coull JT, Vidal F, Nazarian B, Macar F. 2004. Functional anatomy of the attentional modulation of time estimation. Science. 303:1506–1508.
Culham JC, Valyear KF. 2006. Human parietal cortex in action. Curr Opin Neurobiol. 16:205–212.
Damoiseaux JS, Greicius MD. 2009. Greater than the sum of its parts: a review of studies combining structural connectivity and resting-state functional connectivity. Brain Struct Funct. 213:525–533.
Dehaene S, Molko N, Cohen L, Wilson A. 2004. Arithmetic and the brain. Curr Opin Neurobiol. 14:218–224.
Dehaene S, Spelke E, Pinel P, Stanescu R, Tsivkin S. 1999. Sources of mathematical thinking: behavioral and brain-imaging evidence. Science. 284:970–974.
Delazer M, Domahs F, Bartha L, Brenneis C, Lochy A, Trieb T, Benke T. 2003. Learning complex arithmetic—an fMRI study. Brain Res Cogn Brain Res. 18:76–88.
Di Martino A, Scheres A, Margulies DS, Kelly AM, Uddin LQ, Shehzad Z, Biswal B, Walters JR, Castellanos FX, Milham MP. 2008. Functional connectivity of human striatum: a resting state fMRI Study. Cereb Cortex. 18:2735–2747.
Di Martino A, Shehzad Z, Kelly C, Roy AK, Gee DG, Uddin LQ, Gotimer K, Klein DF, Castellanos FX, Milham MP. 2009. Relationship between cingulo-insular functional connectivity and autistic traits in neurotypical adults. Am J Psychiatry. 166:891–899.
Dougherty RF, Ben-Shachar M, Bammer R, Brewer AA, Wandell BA. 2005. Functional organization of human occipital-callosal fiber tracts. Proc Natl Acad Sci USA. 102:7350–7355.
Duffau H, Denvil D, Lopes M, Gasparini F, Cohen L, Capelle L, Van Effenterre R. 2002. Intraoperative mapping of the cortical areas involved in multiplication and subtraction: an electrostimulation study in a patient with a left parietal glioma. J Neurol Neurosurg Psychiatry. 73:733–738.
Egner T, Monti JM, Trittschuh EH, Wieneke CA, Hirsch J, Mesulam MM. 2008. Neural integration of top-down spatial and feature-based information in visual search. J Neurosci. 28:6141–6151.
Eickhoff SB, Stephan KE, Mohlberg H, Grefkes C, Fink GR, Amunts K, Zilles K. 2005. A new SPM toolbox for combining probabilistic cytoarchitectonic maps and functional imaging data. Neuroimage. 25:1325–1335.
Etkin A, Keller KE, Schatzberg AF, Menon V, Greicius MD. 2009. Disrupted amygdalar subregion functional connectivity and evidence for a compensatory network in generalized anxiety disorder. Arch Gen Psychiatry. 66:1361–1372.
Fox MD, Corbetta M, Snyder AZ, Vincent JL, Raichle ME. 2006. Spontaneous neuronal activity distinguishes human dorsal and ventral attention systems. Proc Natl Acad Sci USA. 103:10046–10051.
Fox MD, Snyder AZ, Vincent JL, Raichle ME. 2007. Intrinsic fluctuations within cortical systems account for intertrial variability in human behavior. Neuron. 56:171–184.
Fransson P. 2005. Spontaneous low-frequency BOLD signal fluctuations: an fMRI investigation of the resting-state default mode of brain function hypothesis. Hum Brain Mapp. 26:15–29.
Frey SH, Vinton D, Norlund R, Grafton ST. 2005. Cortical topography of human anterior intraparietal cortex active during visually guided grasping. Brain Res Cogn Brain Res. 23:397–405.
Friston KJ, Frith CD, Frackowiak RS, Turner R. 1995. Characterizing dynamic brain responses with fMRI: a multivariate approach. Neuroimage. 2:166–172.
Goodale MA, Milner AD. 1992. Separate visual pathways for perception and action. Trends Neurosci. 15:20–25.
Grefkes C, Fink GR. 2005. The functional organization of the intraparietal sulcus in humans and monkeys. J Anat. 207:3–17.
Greicius MD, Krasnow B, Reiss AL, Menon V. 2003. Functional connectivity in the resting brain: a network analysis of the default mode hypothesis. Proc Natl Acad Sci USA. 100:253–258.
Greicius MD, Srivastava G, Reiss AL, Menon V. 2004. Default-mode network activity distinguishes Alzheimer's disease from healthy aging: evidence from functional MRI. Proc Natl Acad Sci USA. 101:4637–4642.
Greicius MD, Supekar K, Menon V, Dougherty RF. 2009. Resting-state functional connectivity reflects structural connectivity in the default mode network. Cereb Cortex. 19:72–78.
Gruber O, Indefrey P, Steinmetz H, Kleinschmidt A. 2001. Dissociating neural correlates of cognitive components in mental calculation. Cereb Cortex. 11:350–359.
Habas C, Kamdar N, Nguyen D, Prater K, Beckmann CF, Menon V, Greicius MD. 2009. Distinct cerebellar contributions to intrinsic connectivity networks. J Neurosci. 29:8586–8594.
Hagmann P, Cammoun L, Gigandet X, Meuli R, Honey CJ, Wedeen VJ, Sporns O. 2008. Mapping the structural core of human cerebral cortex. PLoS Biol. 6:e159.
Hew WK, Thomas KJ, Pepper M, Farrer I, Anderson D, Jones GA, Ritchie DA. 2008. Spin-incoherent transport in quantum wires. Phys Rev Lett. 101:036801.
Honey CJ, Sporns O, Cammoun L, Gigandet X, Thiran JP, Meuli R, Hagmann P. 2009. Predicting human resting-state functional connectivity from structural connectivity. Proc Natl Acad Sci USA. 106:2035–2040.
Husain M, Nachev P. 2007. Space and the parietal cortex. Trends Cogn Sci. 11:30–36.
Isaacs E, Edmonds C, Lucas A, Gadian D. 2001. Calculation difficulties in children of very low birthweight: a neural correlate. Brain. 124:1701–1707.
Ischebeck A, Zamarian L, Egger K, Schocke M, Delazer M. 2007. Imaging early practice effects in arithmetic. Neuroimage. 36:993–1003.
Ischebeck A, Zamarian L, Schocke M, Delazer M. 2009. Flexible transfer of knowledge in mental arithmetic–an fMRI study. Neuroimage. 44:1103–1112.
James TW, Culham J, Humphrey GK, Milner AD, Goodale MA. 2003. Ventral occipital lesions impair object recognition but not object-directed grasping: an fMRI study. Brain. 126:2463–2475.

Jones DK. 2004. The effect of gradient sampling schemes on measures derived from diffusion tensor MRI: a Monte Carlo study. Magn Reson Med. 51:807–815.
Jones DK. 2008. Studying connections in the living human brain with diffusion MRI. Cortex. 44:936–952.
Kelly AM, Uddin LQ, Biswal BB, Castellanos FX, Milham MP. 2008. Competition between functional brain networks mediates behavioral variability. Neuroimage. 39:527–537.
Kennedy DP, Courchesne E. 2008. The intrinsic functional organization of the brain is altered in autism. Neuroimage. 39:1877–1885.
Kesler SR, Menon V, Reiss AL. 2006. Neuro-functional differences associated with arithmetic processing in Turner syndrome. Cereb Cortex. 16:849–856.
Li TQ, Takahashi A, Wang Y, Mathews V, Glover GH. 2006. Dual-echo spiral in/in acquisition method for reducing magnetic susceptibility artifacts in blood-oxygen-level-dependent functional magnetic resonance imaging. Magn Reson Med. 55:325–334.
Makin TR, Holmes NP, Zohary E. 2007. Is that near my hand? Multisensory representation of peripersonal space in human intraparietal sulcus. J Neurosci. 27:731–740.
McNab F, Klingberg T. 2008. Prefrontal cortex and basal ganglia control access to working memory. Nat Neurosci. 11:103–107.
Menon V, Rivera SM, White CD, Glover GH, Reiss AL. 2000. Dissociating prefrontal and parietal cortex activation during arithmetic processing. Neuroimage. 12:357–365.
Mesulam MM. 1998. From sensation to cognition. Brain. 121(Pt 6):1013–1052.
Mesulam MM, Mufson EJ. 1982. Insula of the old world monkey. III: Efferent cortical output and comments on function. J Comp Neurol. 212:38–52.
Molko N, Cachia A, Rivière D, Mangin J, Bruandet M, Le Bihan D, Cohen L, Dehaene S. 2003. Functional and structural alterations of the intraparietal sulcus in a developmental dyscalculia of genetic origin. Neuron. 40:847–858.
Mori S. 2007. Introduction to Diffusion Tensor Imaging. Amsterdam: Elsevier.
Mori S, Crain BJ, Chacko VP, van Zijl PC. 1999. Three-dimensional tracking of axonal projections in the brain by magnetic resonance imaging. Ann Neurol. 45:265–269.
Nieder A, Dehaene S. 2009. Representation of number in the brain. Annu Rev Neurosci. 32:185–208.
Pajevic S, Aldroubi A, Basser PJ. 2002. A continuous tensor field approximation of discrete DT-MRI data for extracting microstructural and architectural features of tissue. J Magn Reson. 154:85–100.
Petrides M, Pandya DN. 2009. Distinct parietal and temporal pathways to the homologues of Broca's area in the monkey. PLoS Biol. 7:e1000170.
Piazza M, Pinel P, Le Bihan D, Dehaene S. 2007. A magnitude code common to numerosities and number symbols in human intraparietal cortex. Neuron. 53:293–305.
Price G, Holloway I, Räsänen P, Vesterinen M, Ansari D. 2007. Impaired parietal magnitude processing in developmental dyscalculia. Curr Biol. 17:R1042–R1043.
Raichle ME, MacLeod AM, Snyder AZ, Powers WJ, Gusnard DA, Shulman GL. 2001. A default mode of brain function. Proc Natl Acad Sci USA. 98:676–682.
Rosenberg-Lee M, Tsang J, Menon V. 2009. Symbolic, numeric, and magnitude representations in the parietal cortex. Commentary on R. Cohen Kadosh and V. Walsh, Numerical representation in the parietal lobes: abstract or not abstract? Behav Brain Sci. 32:350–351.
Rotzer S, Kucian K, Martin E, von Aster M, Klaver P, Loenneker T. 2008. Optimized voxel-based morphometry in children with developmental dyscalculia. Neuroimage. 39:417–422.
Rushworth MF, Behrens TE, Johansen-Berg H. 2006. Connection patterns distinguish 3 regions of human parietal cortex. Cereb Cortex. 16:1418–1430.
Seeley WW, Crawford RK, Zhou J, Miller BL, Greicius MD. 2009. Neurodegenerative diseases target large-scale human brain networks. Neuron. 62:42–52.
Seeley WW, Menon V, Schatzberg AF, Keller J, Glover GH, Kenna H, Reiss AL, Greicius MD. 2007. Dissociable intrinsic connectivity networks for salience processing and executive control. J Neurosci. 27:2349–2356.
Sherbondy AJ, Dougherty RF, Napel S, Wandell BA. 2008. Identifying the human optic radiation using diffusion imaging and fiber tractography. J Vis. 8:12.1–12.11.
Shulman GL, Astafiev SV, Franke D, Pope DL, Snyder AZ, McAvoy MP, Corbetta M. 2009. Interaction of stimulus-driven reorienting and expectation in ventral and dorsal frontoparietal and basal ganglia-cortical networks. J Neurosci. 29:4392–4407.
Shulman GL, Fiez JA, Corbetta M, Buckner RL, MMF, Raichle ME, Petersen SE. 1997. Common blood flow changes across visual tasks: II. Decreases in cerebral cortex. J Cogn Neurosci. 9:648–663.
Skudlarski P, Jagannathan K, Calhoun VD, Hampson M, Skudlarska BA, Pearlson G. 2008. Measuring brain connectivity: diffusion tensor imaging validates resting state temporal correlations. Neuroimage. 43:554–561.
Squire LR. 2009. Memory and brain systems: 1969–2009. J Neurosci. 29:12711–12716.
Sridharan D, Levitin DJ, Chafe CH, Berger J, Menon V. 2007. Neural dynamics of event segmentation in music: converging evidence for dissociable ventral and dorsal networks. Neuron. 55:521–532.
Stuss DT, Gallup GG, Jr., Alexander MP. 2001. The frontal lobes are necessary for 'theory of mind'. Brain. 124:279–286.
Supekar K, Menon V, Rubin D, Musen M, Greicius MD. 2008. Network analysis of intrinsic functional brain connectivity in Alzheimer's disease. PLoS Comput Biol. 4:e1000100.
Uddin LQ, Kelly AM, Biswal BB, Xavier Castellanos F, Milham MP. 2009. Functional connectivity of default mode network components: correlation, anticorrelation, and causality. Hum Brain Mapp. 30:625–637.
Uddin LQ, Mooshagian E, Zaidel E, Scheres A, Margulies DS, Kelly AM, Shehzad Z, Adelstein JS, Castellanos FX, Biswal BB, et al. 2008. Residual functional connectivity in the split-brain revealed with resting-state functional MRI. Neuroreport. 19:703–709.
van den Heuvel M, Mandl R, Luigjes J, Hulshoff Pol H. 2008. Microstructural organization of the cingulum tract and the level of default mode functional connectivity. J Neurosci. 28:10844–10851.
van den Heuvel MP, Mandl RC, Kahn RS, Hulshoff Pol HE. 2009. Functionally linked resting-state networks reflect the underlying structural connectivity architecture of the human brain. Hum Brain Mapp. 30:3127–3141.
Vincent JL, Snyder AZ, Fox MD, Shannon BJ, Andrews JR, Raichle ME, Buckner RL. 2006. Coherent spontaneous activity identifies a hippocampal-parietal memory network. J Neurophysiol. 96:3517–3531.
Vogel EK, McCollough AW, Machizawa MG. 2005. Neural measures reveal individual differences in controlling access to working memory. Nature. 438:500–503.
Wu SS, Chang TT, Majid A, Caspers S, Eickhoff SB, Menon V. 2009. Functional heterogeneity of inferior parietal cortex during mathematical cognition assessed with cytoarchitectonic probability maps. Cereb Cortex. 19:2930–2945.
Xu Y, Chun MM. 2009. Selecting and perceiving multiple visual objects. Trends Cogn Sci. 13:167–174.